Steel and Composite Structures, *Vol. 35, No. 1 (2020) 93-109*
DOI: https://doi.org/10.12989/scs.2020.35.1.093

Numerical study of concrete-encased CFST under preload followed by sustained service load

Gen Li[1], Chao Hou*[2], Lin-Hai Han[3] and Luming Shen[1]

[1]School of Civil Engineering, The University of Sydney, Sydney, NSW 2006, Australia
[2]Department of Ocean Science and Engineering, Southern University of Science and Technology, Shenzhen, 518055, P. R. China
[3]Department of Civil Engineering, Tsinghua University, Beijing, 100086, P. R. China

(*Received January 15, 2020, Revised February 20, 2020, Accepted February 22, 2020*)

Abstract. Developed from conventional concrete filled steel tubular (CFST) members, concrete-encased CFST has attracted growing attention in building and bridge practices. In actual construction, the inner CFST is erected prior to the casting of the outer reinforced concrete part to support the construction preload, after which the whole composite member is under sustained service load. The complex loading sequence leads to highly nonlinear material interaction and consequently complicated structural performance. This paper studies the full-range behaviour of concrete-encased CFST columns with initial preload on inner CFST followed by sustained service load over the whole composite section. Validated against the reported data obtained from specifically designed tests, a finite element analysis model is developed to investigate the detailed structural behaviour in terms of ultimate strength, load distribution, material interaction and strain development. Parametric analysis is then carried out to evaluate the impact of significant factors on the structural behaviour of the composite columns. Finally, a simplified design method for estimating the sectional capacity of concrete-encased CFST is proposed, with the combined influences of construction preload and sustained service load being taken into account. The feasibility of the developed method is validated against both the test data and the simulation results.

Keywords: concrete-encased CFST; construction preload; sustained service load; numerical analysis; sectional capacity

1. Introduction

For decades, steel-concrete composite structures have been widely recognized since they can effectively make use of the structural properties of each material and are thus competitive in strength, stiffness, ductility, energy absorption capacity and construction speed when compared with traditional reinforced concrete (RC) structures (Han *et al*. 2014, Varma *et al*. 2002, Lam and Williams 2004, Kang *et al*. 2015). Consisting of an inner concrete filled steel tube (CFST) component and an outer RC component, concrete-encased CFST is a novel kind of composite structure which is emerging as the main load-carrying members in high-rise buildings and long-span bridge constructions (Ma *et al*. 2019). When comparing a concrete-encased CFST member to a reference conventional CFST, the outer RC component of the former effectively contributes to the increased anti-corrosion performance as well as fire resistance (Campian *et al*. 2015). Meanwhile, the confinement actions between the outer RC and the inner CFST greatly benefit the cross-sectional capacity and rigidity of the member.

In recent years, there are increasing research reports on the structural performance of concrete-encased CFST. Previously, research investigations were mainly conducted on the static performance of such novel composite members under compression (Han and An 2014), tension (Han *et al*. 2016), and compression combined with torsion (Li *et al*. 2018). Furthermore, studies in terms of the dynamic performance (Ma *et al*. 2018a, Zhang *et al*. 2018) and the fire performance (Zhou and Han 2018) showed that the concrete-encased CFST members exhibited better performance in regard of ductility and fire resistance than the conventional CFSTs, which was mainly attributed to the surrounding RC and its confinement on the inner CFST.

In the construction practices of a concrete-encased CFST building, the inner CFST component usually acts as the vertical skeleton framework to reduce the propping cost and the time consumption during the construction stage, with the typical construction sequence of the main composite column illustrated in Fig. 1 (Li *et al*. 2019). Therefore, the inner CFST is normally erected before the outer RC component, and it thus bears alone the self-weight of upper structures as well as the load caused by construction activities on site. As pointed out in Li *et al*. (2015), these construction loads would cause prior stress and deformation to the earlier formed structural component and change the deformation compatibility state, and the bearing capacity of the overall composite member would consequently be affected. Previously, several research studies on the performance of conventional composite columns with the construction preload effect considered have been conducted (Han and Yao 2003, Wu *et al*. 2012, Uy and Das 1997), where it was found that the effects of preload were non-negligible and the wet concrete loading sometimes governed the slenderness limits of priory erected

*Corresponding author, Ph.D.
E-mail: houc@sustech.edu.cn

http://www.techno-press.org/?journal=scs&subpage=8
ISSN: 1598-9367 (Print), 1598-6233 (Online)

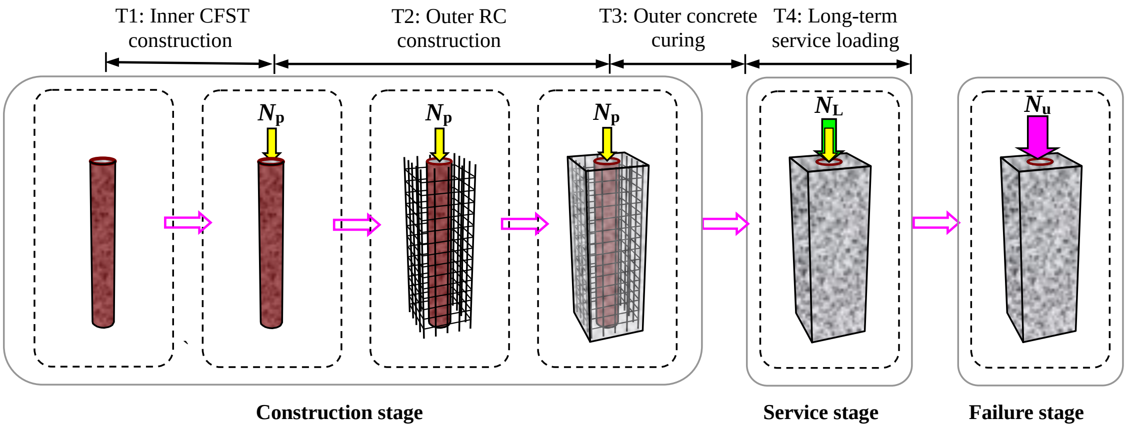

Fig. 1 Life-cycle stages of concrete-encased CFST columns including the construction process (Li *et al*. 2019)

steel plates. Eight CFST columns were tested by Liew and Xiong (2009) with preload on the steel tubes, leading to a modification based on Eurocode 4 to predict the axial strength of the columns with preloads. Li *et al*. (2012) developed a finite element analysis (FEA) model to simulate the preload on concrete filled double skin tubular (CFDST) columns, with a formula proposed to quantify the influence of preload on the corresponding sectional capacity.

Since the fully constructed composite columns are under sustained service load in the service stage of a building, another critical factor that might affect the material interaction and load distribution within the column is the intrinsic long-term time dependent behaviour of concrete. Shrinkage and creep of concrete will cause issues including additional deformation, stress concentration and internal force redistribution along the composite cross-section through deformation compatibility. Some researchers presented investigations on the long-term behaviour of conventional composite structures under sustained load (e.g., Yang *et al*. 2015, Ichinose *et al*. 2001, Han *et al*. 2011). In a concrete-encased CFST, the fact that the confinement conditions of the concrete vary at the inner or outer regions of the steel tube makes the long-term effects even more complicated. Moreover, the outer concrete is directly exposed in an atmospheric environment, while the inner concrete core is under an airtight condition, resulting in long-term performance differences which need to be considered. Ma *et al*. (2018b) established a FEA model to evaluate the impacts of sustained load on the structural performance of concrete-encased CFST columns, and proposed a relevant strength index to account for the long-term effects. Besides this, limited studies are available regarding the long-term performance of this new composite column.

Due to the unique configuration and construction sequence of concrete-encased CFST columns, the combined effects of construction preload followed by sustained service load are critical to the ultimate strength and the full-range structural performance. To rationally address this issue, a set of experimental tests have been reported by the authors (2019), where 14 composite columns were tested under the reproduced construction and loading sequence. It was found that the combined loading has non-negligible negative effects on the sectional capacity, the stiffness and the column ductility. However, since available test data is very limited and the scope of parameters need to be extended, there is still a necessity of effective numerical approaches and in-depth analytical studies. Therefore, this paper presents the analytical behaviour of concrete-encased CFST columns with construction preload on the inner CFST followed by sustained service load on the entire cross-section. The main objectives include: 1) To present a numerical model for concrete-encased CFST column under construction preload followed by sustained service load. The FEA model will be able to consider different confinement and long-term effects for materials in different components of the composite column, and will be thoroughly validated against test data; 2) To perform full-range analysis on the structural behaviour of the composite column with combined construction preload and sustained service load in terms of sectional capacity, load distribution, nonlinear material interaction and strain development; 3) To conduct extended parametric analysis on the effects of important factors including the material strengths, the cross-sectional configuration, and the initial loading ratios; 4) To propose a simplified design formula for calculating the sectional capacity of concrete-encased CFST columns with construction preload on the inner CFST followed by sustained service load over the entire composite section. The feasibility of the design method is validated against both the experimental data and the numerical simulation.

2. Finite element analysis (FEA) modelling

2.1 Element type and meshing

The numerical analysis was conducted by employing the commercial finite element analysis package ABAQUS/Standard module (2016). A general view of the developed model for a concrete-encased CFST specimen is exhibited in Fig. 2. The loading endplates as well as all the concrete components, namely the outer concrete and the concrete core, were simulated by three dimensional eight-node brick elements with reduced integration (C3D8R).

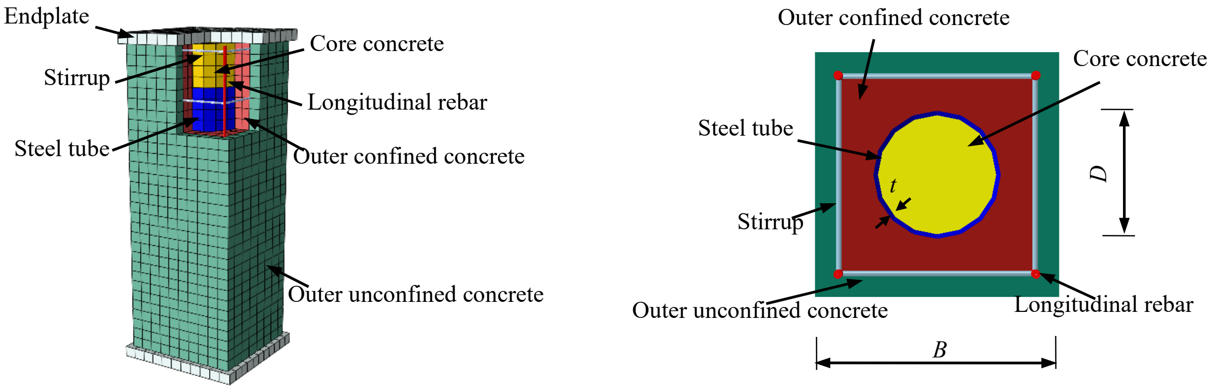

(a) Schematic view (b) Section view

Fig. 2 Schematic view of the FEA model for concrete-encased CFST column

(a) Core concrete (b) Outer concrete

Fig. 3 Stress (σ) - strain (ε) relation of concrete materials

For steel components, the tube was modelled by four-node shell elements with reduced integration (S4R) while two-node truss elements (T3D2) were assigned for the longitudinal rebars and the stirrups. A suitable mesh density computational efficiency was obtained by performing the mesh convergence study. The selected dimensions of elements were generally identical in all three directions, i.e., 20 mm, as shown in Fig. 2(a).

2.2 Material properties

Elasto-plastic models were employed to represent the constitutive relationships of the steel components since the sustained service load has little influence on the performance of steel. For the steel tube, a five-stage stress-strain model put forward in Han *et al.* (2007) which could well capture the elasto-plastic response of a steel tube was adopted as the uniaxial stress-strain relationship. For the longitudinal rebars and the stirrups, a bilinear stress-strain model was adopted in the modelling, where a modulus of $0.01E_s$ was applied to account for the strain hardening effect, with E_s being the initial elastic modulus. Moreover, the steel endplates were modelled as rigid blocks with infinite stiffness so that the deformation can be ignored.

A proper consideration of constitutive behaviour for concrete components is one of the key elements for a successful simulation of concrete-encased CFST. The concrete damage plasticity (CDP) model was used to describe the constitutive behaviour of concrete. According to different confinement states inside a concrete-encased CFST, the concrete materials along the entire cross-section can be classified into three categories, i.e., the concrete core confined by the steel tube, the outer concrete confined by the stirrups and the outer unconfined concrete cover, as highlighted in Fig. 2(b) using different colours. For the concrete core, an uniaxial compressive constitutive model well recognized for its effectiveness in simulating the confined concrete within a steel tube. For the outer concrete cover with no confinement, the stress-strain relation suggested by Attard and Setunge (1996) was utilized to represent the constitutive performance. For the outer confined concrete between the steel tube and the stirrups, the stress-strain relationship suggested by Han and An (2014) was adopted to describe the increased plasticity attributed to the restraint provided by the stirrups. Fig. 3 exhibits the above determined stress-strain curves for concrete components under different confinement conditions, from which it can be observed that the plasticity enhancement of the concrete material can be achieved by the confinement. To describe the tensile softening behaviour of concrete, the fracture energy model proposed by Hillerborg *et al.* (1976) was adopted.

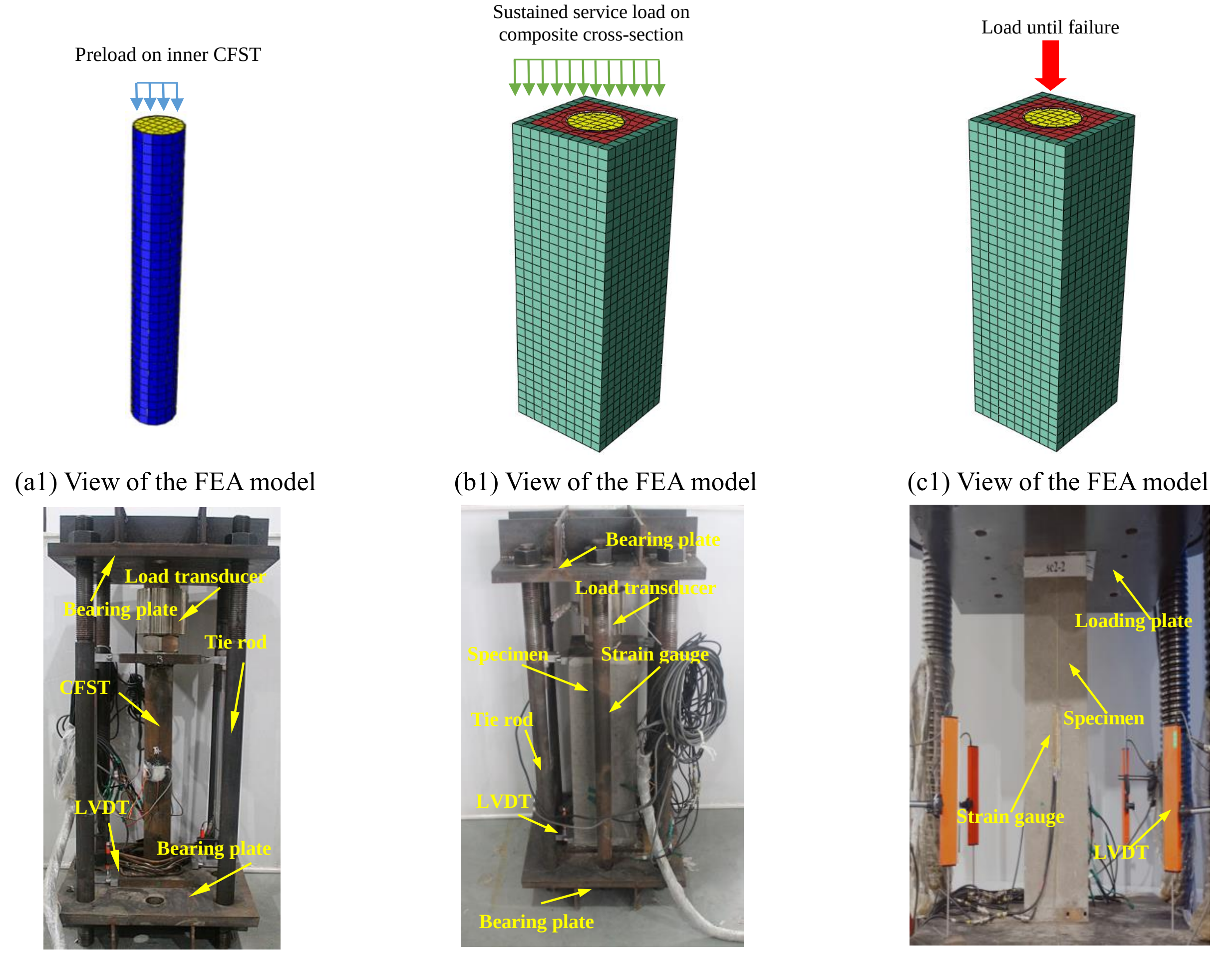

(a1) View of the FEA model (b1) View of the FEA model (c1) View of the FEA model

(a2) Test setup (Li *et al*. 2019) (b2) Test setup (Li *et al*. 2019) (c2) Test setup (Li *et al*. 2019)

(a) Preload stage (b) Sustained load stage (c) Sectional capacity test stage

Fig. 4 Loading sequence of the concrete-encased CFST columns

As suggested in Chu and Carreia (1986), the long-term effects of concrete material could be accounted for by modifying the short-term constitutive model developed by Han *et al*. (2007) was adopted, which has been using the selected creep coefficients, the feasibility of which has been validated in many previous research (Han *et al*. 2011, Ma *et al*. 2018b). Thus, the method was employed here as well to consider the effect of sustained service load on the concrete behaviour during the service stage, i.e., adjusting the concrete strain by multiplying a factor of (1+ϕ_u) while maintaining the concrete stress unchanged under the sustained load, where the creep coefficient ϕ_u was determined according to the test results in Li *et al*. (2019).

2.3 Material interaction and boundary conditions

Unlike the case in a conventional CFST, contact interfaces between steel and concrete exist at both the inner and outer surfaces of the tube inside a concrete-encased CFST. "Surface-to-surface" contact interaction was assigned to the two steel-concrete interfaces. At these interfaces, "Hard contact" was set to allow separation whilst restraining the penetration of the contact surfaces. A Coulomb friction model was employed tangentially with a friction coefficient defined according to the contacted materials and the treatment of the interface, i.e., 0.6 in this study as suggested in Han *et al*. (2007). A set of push-out tests on concrete-encased CFST were carried out by Han *et al*. (2016) to study the bond performance, where an average bond strength (τ_{bond}) of 3.63 MPa was obtained between the steel tube and the outer concrete. This research outcome was adopted in current modelling as well. As for the bond strength between the tube and the inner concrete core, it was estimated by employing the following equation proposed in Roeder *et al*. (1999).

$$\tau_{\text{bond}} = 2.314 - 0.0195(D/t) \quad \text{(MPa)} \tag{1}$$

where D is the outer diameter of the steel tube in concrete-encased CFST, and t is the tubular thickness. The "Tie" constraint was adopted for all the contacts associated with the endplates including the outer and inner concrete, the steel tube and the longitudinal rebars. In addition, the longitudinal reinforcements and the stirrups were "Embedded" in the outer concrete. Consistent with the testing program in the companion paper (2019), both the top and the bottom endplates were fixed except for the longitudinal displacement of the top endplate to allow the load to be applied.

2.4 Simulation of the construction preload and the sustained service load

To simulate a typical loading sequence of a concrete-encased CFST column in practice, four loading steps were created in the FEA analysis to simulate the three loading stages shown in Fig. 4. The three loading stages included the preload stage exhibited in Fig. 4(a), the sustained loading stage shown in Fig. 4(b) and the sectional capacity test stage shown in Fig. 4(c). This was in accordance with the experimental program in Li *et al*. (2019), with the photos of the corresponding test setup shown in Fig. 4 as well. A brief description of the four loading steps is given as follows.

- Loading step 1: application of the preload. In the first step, the outer RC component was set as deactivated whilst applying a specified preload on the inner CFST only, as shown in Fig. 4(a1). This was to simulate the actual construction stage when the outer RC was not formed yet and the inner CFST carried the construction load as an individual structural member.
- Loading step 2: formation of the entire composite specimen and application of the sustained service load. At the beginning of this step, the outer RC component was activated by editing the ABAQUS input file using the "Model change" keyword. This would activate the outer RC component together with its interactions with the inner CFST, i.e., to simulate the casting of the outer RC in practice and the formation of the concrete-encased CFST column. In this way, both the outer RC and the inner CFST components would bear together the sustained service load applied on the overall composite section, as shown in Fig. 4(b1). During this step, the existing preload was increased to the specified value of the sustained service load.
- Loading step 3: maintaining of the sustained service load and consideration of the long-term effects. As introduced in Section 2.2, the time-dependent effects of concrete were considered within this step by modifying the concrete constitutive models to account for the creep deformation and the variation of material modulus. It should be noted that, given the fact that the confinement conditions vary among concrete components in different regions of the section, different creep coefficients were used for the outer and inner concrete, based on the test results in Li *et al.* (2019).
- Loading step 4: application of continued loading until the failure of the columns. During this step, the load was continued using the displacement controlled load at the top endplate until the concrete-encased CFST columns failed. The peak load was considered as the sectional capacity of the column, and the column was considered failure when the load further dropped to 85% of the sectional capacity. The loading was then terminated.

2.5 Verification of the FEA modelling

The test results of concrete-encased CFST under initial preload followed by sustained load reported by the authors (Li *et al*. 2019), together with the collected data from the previously reported axial compressive tests on eight concrete-encased CFST stub columns (Chen *et al*. 2002), were adopted to validate the established model. Information of the specimens tested in Li *et al*. (2019) is summarized in Table 1, where B represents the side length of the concrete-encased CFST section, illustrated in Fig. 2(b); l represents the overall column length; D and t represent the steel tubular diameter and thickness, respectively, as illustrated in Fig. 2(b); f_y represents the yield strength of steel tube; $f_{cu,core}$ and $f_{cu,out}$ represent the cube strengths of the inner and the outer concrete, respectively; n_p and n_l represent the construction preload ratio and the service load ratio, respectively.

The construction preload ratio n_p is calculated as the preload N_P on the inner CFST over the sectional capacity of the CFST component, while the sustained service load ratio n_l is calculated as the sustained service load N_L over the sectional capacity of the concrete-encased CFST column. Further details of the tested specimens can be obtained in Li *et al*. (2019).

Verification of the FEA modelling was conducted in the fields of failure patterns, load-strain relationships and sectional capacity predictions. Fig. 5 presents the comparison between the simulated and tested failure patterns of concrete-encased CFST under construction preload followed by sustained service load.

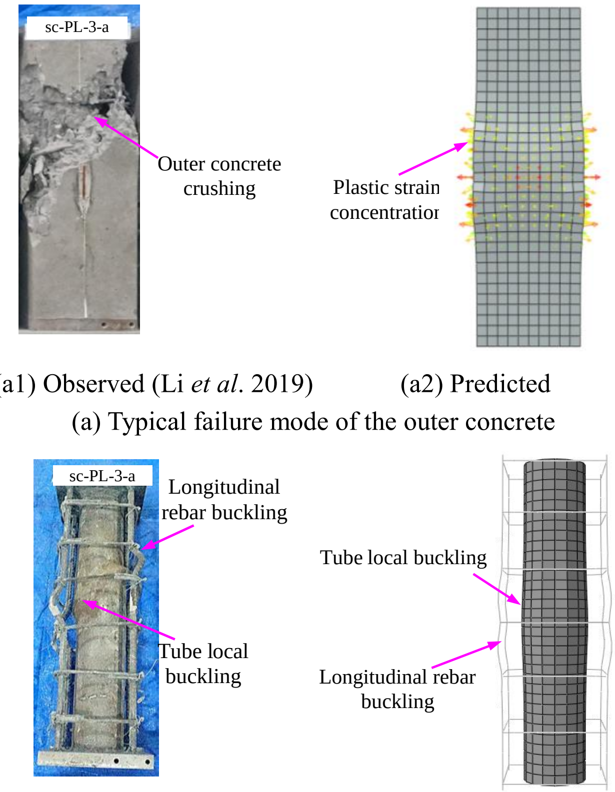

(a1) Observed (Li *et al*. 2019) (a2) Predicted

(a) Typical failure mode of the outer concrete

(b1) Observed (Li *et al*. 2019) (b2) Predicted

(b) Typical failure mode of the steel tube and reinforcement

Fig. 5 Comparison of the predicted and observed failure pattern

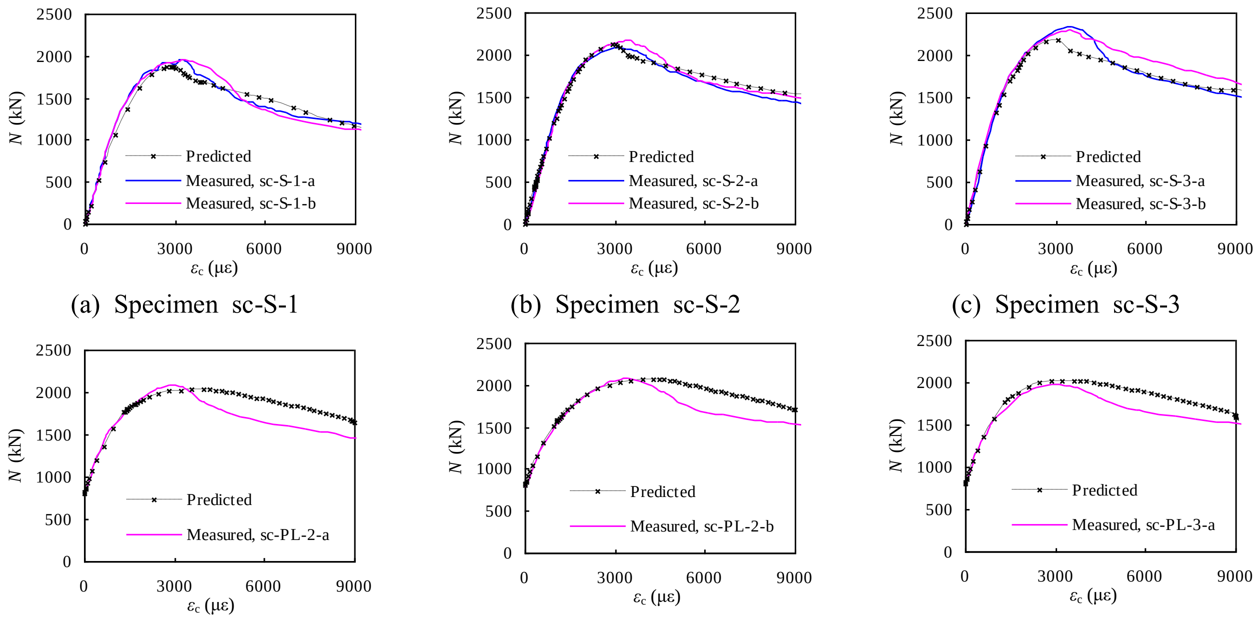

(a) Specimen sc-S-1 (b) Specimen sc-S-2 (c) Specimen sc-S-3

(d) Specimen sc-PL-2-a (e) Specimen sc-PL-2-b (f) Specimen sc-PL-3-a

Fig. 6 Comparison of the predicted and measured N-ε_c relationships at sectional capacity test stages

Given the fact that the detailed cracking pattern of concrete is difficult to be perfectly simulated through the FEA, the maximum principal plastic strain distributions are adopted to reflect the crushed regions in the outer concrete of a concrete-encased CFST. Similar approach has been adopted in previous numerical studies on concrete-encased CFST and proved feasible (Ma *et al*. 2018b, Li *et al*. 2018). It can be observed clearly from Figs. 5(a1) and (a2) that the predicted plastic strain concentration of the outer concrete was generally consistent with the crushed region in the test. The slight differences between the predicted and observed failure patterns may be attributed to the initial imperfection of the materials and the potential eccentricity in the loading setup. Since the current research mainly focuses on the preload effect towards the column ultimate state, the existing differences are considered acceptable. After removing the outer concrete, the outward buckling of the tube, as well as the local buckling of the longitudinal rebars, could be observed in both the predicted and observed patterns, as shown in Figs. 5(b1) and (b2).

The typical load (N) versus axial strain (ε_c) relationships of concrete-encased CFST columns in the sectional capacity test stage are displayed in Fig. 6, where the measured axial strain is obtained by using the column axial shortening, i.e., measured by Linear Variable Differential Transformers (LVDT), over the original column length, while the predicted axial strain is calculated by using the displacement of the top endplate in the axial direction over the original column length. In general, the predicted curves agree with the measured curves in both ultimate strength and column stiffness.

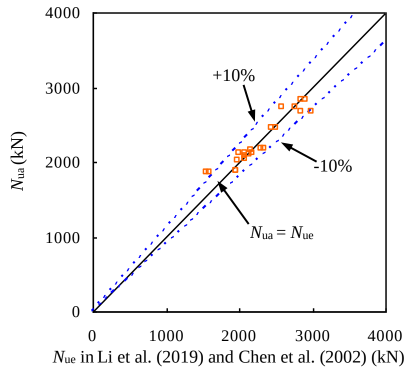

Fig. 7 Comparison of the predicted (N_{ua}) and measured (N_{ue}) sectional capacity

As introduced before, the construction preload and sustained service load were applied prior to the sectional capacity test. Therefore, in the N-ε_c curves in Fig. 6, the load value started from that of the service load and the corresponding axial strain was set to zero at the start of sectional capacity test stage. The peak load of a concrete-encased CFST was taken as the sectional capacity N_u. The predicted capacities using FEA (N_{ua}) of the tested 14 concrete-encased CFST specimens in Li *et al.* (2019) are presented in Table 1 and compared with the corresponding measured values (N_{ue}). The mean value and the standard deviation of the ratio N_{ua}/N_{ue} were 1.013 and 0.077, respectively, indicating satisfactory prediction results. Fig. 7 further displays the comparison between N_{ua} and N_{ue} for a total of 22 specimens collected from Li *et al.* (2019) and

Table 1 Prediction and calculation of the concrete-encased CFST specimens tested in Li *et al*. (2019)

Specimen labels	Overall dimension $B \times l$ (mm)	Inner steel tube $D \times t$ (mm)	f_y (MPa)	$f_{cu,core}$ (MPa)	$f_{cu,outer}$ (MPa)	n_p	n_l	N_{ue} (kN)	N_{ua} (kN)	$N_{uc,PL}$ (kN)	N_{ua}/N_{ue}	$N_{uc,PL}/N_{ue}$	$N_{uc,PL}/N_{ua}$
sc-PL-1-a	200×600	74.3×1.99	356	75.5	44.1	0.3	0.6	1561.5	1862.2	1761.5	1.193	1.128	0.946
sc-PL-1-b	200×600	74.3×1.99	356	75.5	44.1	0.6	0.6	1599.7	1870.3	1756.5	1.169	1.098	0.939
sc-PL-2-a	200×600	101.4×3.12	307	75.5	44.1	0.3	0.6	2086.8	2037.3	1987.0	0.976	0.952	0.975
sc-PL-2-b	200×600	101.4×3.12	307	75.5	44.1	0.6	0.6	2077.9	2072.8	1981.0	0.998	0.953	0.956
sc-PL-3-a	200×600	101.4×3.12	307	75.5	44.1	0.3	0.6	1988.6	2022.3	1987.0	1.017	0.999	0.983
sc-PL-3-b	200×600	101.4×3.12	307	75.5	44.1	0.6	0.6	2149.9	2105.6	1981.0	0.979	0.921	0.941
sc-PL-4-a	200×600	121.7×2.78	280	75.5	44.1	0.3	0.6	1992.2	2124.5	2043.6	1.066	1.026	0.962
sc-PL-4-b	200×600	121.7×2.78	280	75.5	44.1	0.6	0.6	2157.6	2157.4	2038.2	1.000	0.945	0.945
sc-S-1-a	200×600	74.3×1.99	356	75.5	44.1	--	--	1962.2	1872.5	1988.9	0.954	1.014	1.062
sc-S-1-b	200×600	74.3×1.99	356	75.5	44.1	--	--	1953.0	1872.5	1988.9	0.959	1.018	1.062
sc-S-2-a	200×600	101.4×3.12	307	75.5	44.1	--	--	2081.9	2121.4	2130.3	1.019	1.023	1.004
sc-S-2-b	200×600	101.4×3.12	307	75.5	44.1	--	--	2175.0	2121.4	2130.3	0.975	0.979	1.004
sc-S-3-a	200×600	121.7×2.78	280	75.5	44.1	--	--	2339.2	2174.4	2192.9	0.930	0.937	1.009
sc-S-3-b	200×600	121.7×2.78	280	75.5	44.1	--	--	2303.2	2174.4	2192.9	0.944	0.952	1.009
Mean											1.013	0.996	0.985
Standard deviation											0.077	0.058	0.040

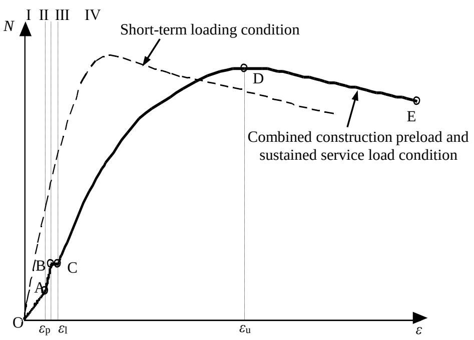

Fig. 8 Typical full-range load (N) versus axial strain (ε_c) relationship of concrete-encased CFST

Chen *et al*. (2002), where good agreement can be observed. Generally, the developed FEA model is demonstrated capable of simulating the concrete-encased CFST columns with initial construction preload on inner CFST followed by sustained service load over the entire composite section.

3. Full-range analysis

The above validated FEA modelling facilitates further studies on the behaviour of the novel composite columns under construction preload followed by sustained service load. A typical concrete-encased CFST column prototype is developed in the FEA model, with the geometric dimensions determined according to the tested samples in the companion paper (Li *et al*. 2019): B = 200 mm, L = 600 mm, D = 100 mm, t = 2.8 mm. Four 12 mm-diameter longitudinal rebars are located at the column corners, while 8 mm diameter stirrups are arranged along the column length with a spacing s = 100 mm and a concrete cover thickness c = 20 mm. The steel tube ratio of the concrete-encased CFST α_s ($=A_s/A_{core}$) = 0.1. Material strengths frequently used in the current practice are adopted in the model: $f_{cu,core}$ = 60 MPa, $f_{cu,out}$ = 40 MPa, and f_y = 345 MPa. It should be noted that according to the common practice, concrete with higher compressive strength is used as the concrete core inside the steel tube for the sake of larger column capacity, while lower strength concrete is used in the outside of the tube to reduce the material cost. This is one of the benefits of casting the concrete components successively rather than simultaneously.

3.1 Load (N) versus axial strain (εc) relationship

According to the experimental observation in Li *et al*. (2019) and the numerical simulation in this study, the combined construction preload and sustained service load have considerable influence on the N-ε_c relationship of such composite columns. The typical full-range N-ε_c curve of the column prototype under construction preload followed by sustained service load, together with the N-ε_c curve of the counterpart subjected to short-term load only is exhibited in Fig. 8. Herein the short-term loading condition refers to the direct displacement-controlled loading till the failure of the column, without any preload or long-term sustained load being considered. As shown from the comparison, when combined loads are applied on a concrete-encased CFST, the overall elastic-plastic behaviour of the column is preserved, whilst considerable changes are detected on the column stiffness, the sectional capacity and the strain corresponding to the sectional capacity. Generally, the N-ε_c curve of a concrete-encased CFST with coupled

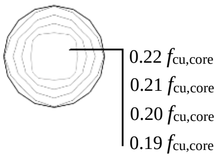

(a) Point A

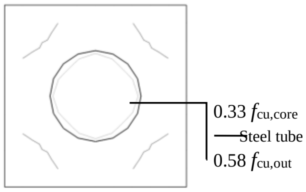

(b) Point B

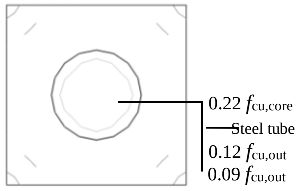

(c) Point C

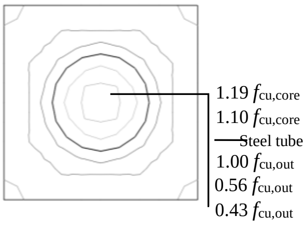

(d) Point D

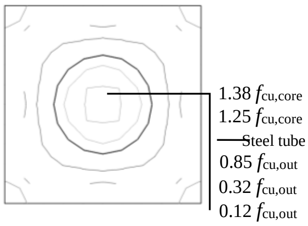

(e) Point E

Fig. 9 Stress distribution of concrete components at characteristic stages of loading

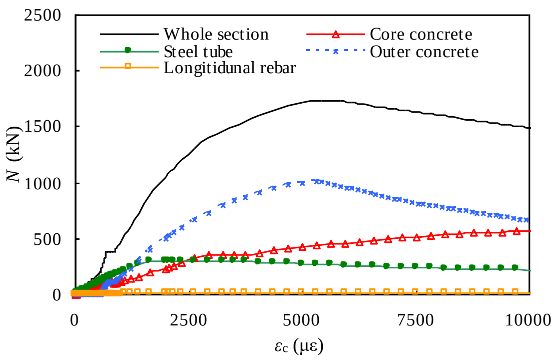

(a) Concrete-encased CFST under combined preload and long-term loading condition

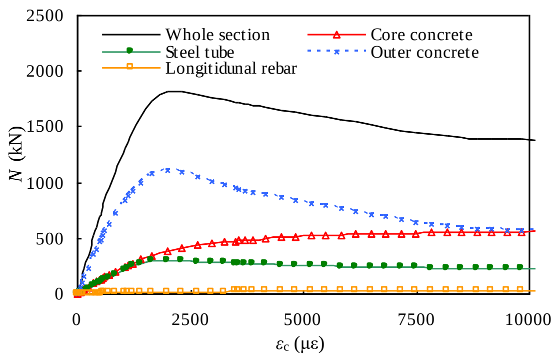

(b) Concrete-encased CFST under short-term loading condition

Fig. 10 Full-range internal force distribution along the composite cross-section

construction preload and sustained service load can be divided into four stages, as illustrated in Fig. 8. The corresponding stress distributions of the concrete materials at the characteristic points A, B, C, D and E along the curve are presented in Fig. 9. It can be observed from Figs. 8 and 9 that:

- Preload stage (Stage I, OA in Fig. 8): The outer RC component is not activated in this stage whilst axial construction preload is applied upon the inner CFST section. According to CECS 188:2008 (2005), a preload level n_p = 0.3 was applied on the prototype to represent normal construction load and structural self-weight. The N-ε_c curve shows elastic behaviour within this stage. At the end of this stage, i.e., Point A, an axial deformation of ε_p is generated for the inner CFST, while the maximum axial stress of the concrete core reaches around 0.22 $f_{cu,core}$ as shown in Fig. 9(a).

- Service load stage (Stage II, AB in Fig. 8): The long-term sustained service load is applied on the whole composite cross-section once the outer RC component is activated at the very beginning of this stage. The sustained service load level is taken as n_l = 0.3 to be comparable with the study in Ma *et al.* (2018b). Since the entire column bears the applied load together in this stage, the corresponding column stiffness becomes much larger than that in Stage I due to the contribution of the RC component, as clearly presented in Fig. 8. The maximum axial stress of the concrete core grows to around 0.33 $f_{cu,core}$ while that of the outer concrete reaches around 0.58 $f_{cu,out}$, as can be seen in Fig. 9(b).

- Long-term sustained load stage (Stage III, BC in Fig. 8): With the long-term load sustained on the composite section, long-term effects of concrete take place, including shrinkage and creep. Therefore, the axial strain increases continuously while the sustained load remains unchanged within this stage. Meanwhile, the time-dependent behaviour of the concrete material leads to load redistribution along the composite cross-section, namely, part of the load carried by concrete is transferred onto the steel tube due to compatibility of deformation. This is clearly observed from Figs. 9(b) and 9(c): compared with the concrete stress values at Point B, at the end of the sustained load stage, i.e., Point C, the maximum axial stress of the inner and outer concrete drop to around 0.22 $f_{cu,core}$ and 0.12 $f_{cu,out}$, respectively.

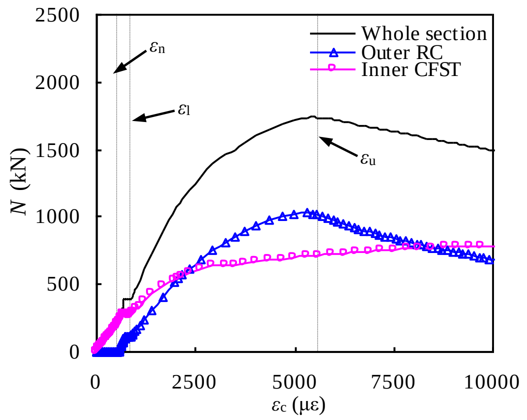

(a1) Full-range N-ε_c curve of the two components

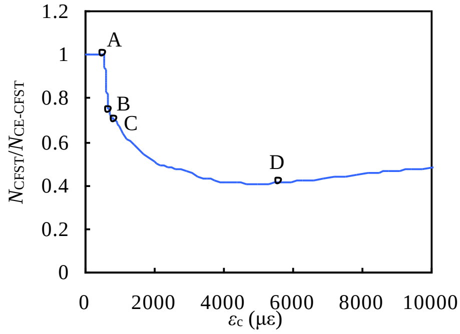

(a2) Full-range $N_{CFST}/N_{CE\text{-}CFST}$ versus ε_c relationship

(a) Combined construction preload and sustained service loading condition

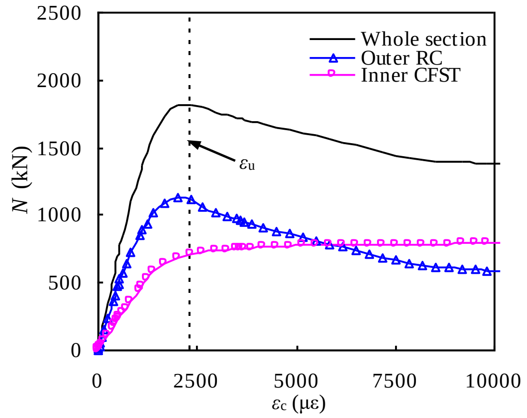

(b1) Full-range N-ε_c curve of the two components

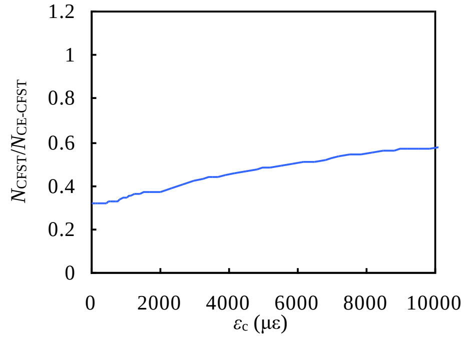

(b2) Full-range $N_{CFST}/N_{CE\text{-}CFST}$ versus ε_c relationship

(b) Short-term loading condition

Fig. 11 Contribution of outer RC and inner CFST components in concrete-encased CFST

- Sectional capacity test stage (Stage IV, CE in Fig. 8): Point E denotes the time when the applied load drops to 85% of the column sectional capacity. The composite column exhibits a clear elasto-plastic behaviour within this stage. The column reaches its sectional capacity N_u at point D, with a corresponding axial deformation of ε_u. Compared with the N-ε_c curve of the short-term loaded counterpart also shown in Fig. 8, there is a certain drop, i.e., 4.8%, in the sectional capacity of the column under the combined load. The stiffness of the latter is obviously smaller than the former due to the effects of both construction preload and sustained service load. Likewise, the strain corresponding to the ultimate strength ε_u is much larger when the combined load is applied. Specifically, ε_u = 5,621 με for the typical column under combined load condition, whilst ε_u = 2,320 με for the short-term loading counterpart. The load starts to fall off after N_u is reached whilst the axial stress of the concrete core keeps increasing, as shown in Figs. 9(d) and 9(e). When the sectional capacity of the composite column drops to 85% of N_u, as exhibited in Fig. 9(e), the longitudinal stress of the outer concrete falls below $0.5f_{cu,out}$, while the maximum stress of the concrete core increases to around $1.38f_{cu,core}$. This is based on the fact that the outer concrete begins to crush when reaching the sectional capacity, while the steel tube continuous to provide confinement to the concrete core, leading to enhanced compressive capacity of the latter which can then be reflected in the FEA modelling when adopting the material constitutive model suggested by Han *et al*. (2007).

3.2 Internal force distribution

The simulated full-range load distribution among the various components of a concrete-encased CFST column under construction preload followed by sustained service load is presented in Fig. 10(a), where the axial loads carried by the concrete core, the steel tube, the outer concrete and the longitudinal rebars are exhibited separately. For comparison, the internal load distribution of the reference short-termly loaded column is displayed in Fig. 10(b).

Generally, the load distribution among various components of the columns shows a similar trend for specimens with and without combined load. The axial load resisted by different components continuously increases before reaching the sectional capacity of the specimens.

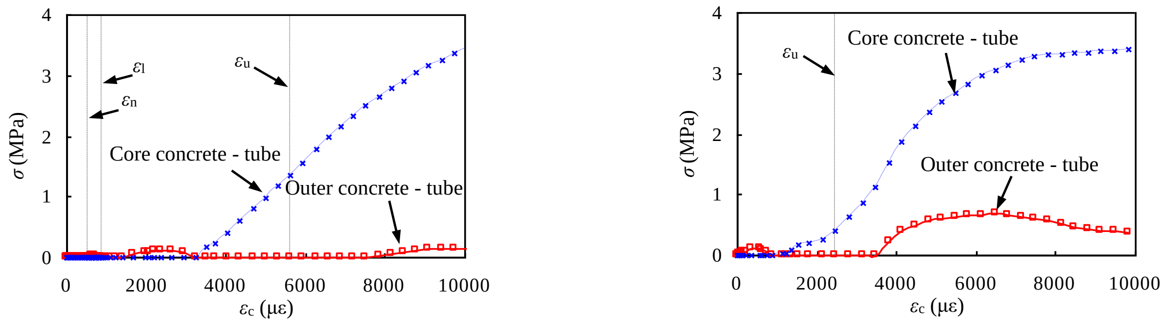

(a) Combined construction preload and sustained service loading condition

(b) Short-term loading condition

Fig. 12 Development of the contact stress (p) in concrete-encased CFST

When the sectional capacity is reached, the outer concrete undertakes 56.4% and 59.9% of the axial load for columns with and without the combined load, respectively. The outer concrete undertakes more than 50% of the axial load, which is attributed to its larger cross-sectional area. Afterwards, the crushing of outer concrete develops and leads to reduced load resisted by this part, while that of the concrete core keeps increasing because of the effective confinement from the tube, which is consistent with the observation from the full-range load-strain analysis presented in Fig. 9. It should be noticed that, due to the long-term effects, the outer concrete under combined loading has a smaller stiffness than that under short-term loading condition. As can be seen from Fig. 10(a), during the long-term sustained load stage, the load resisted by both the inner and outer concrete component drop continuously, whilst the load carried by the steel tube increases correspondingly. This again proves that the time-dependent property of the concrete material results in load redistribution, prompting the steel tube to take over part of the load resisted by the concrete, i.e., around 30% in this prototype case, due to the deformation compatibility.

Based on the analysis, the loads resisted by the outer RC and the inner CFST components during the whole loading stage are calculated and exhibited in Fig. 11. The overall proportion of the force carried by the inner CFST, i.e., $N_{CFST}/N_{CE\text{-}CFST}$, is also presented in Figs. 11(a2) and (b2) for the two loading conditions. From the observations of both cases, the inner CFST contributes significantly to the ductility of the overall column because the outer RC starts to lose its load-carrying capacity after crushing occurs. Meanwhile, the effects of the combined loads on the load-transferring mechanism are clearly shown in Figs. 11(a1) and (a2). Since the preload is resisted by the inner CFST only prior to the formation of the outer RC, $N_{CFST}/N_{CE\text{-}CFST}$ equals 1.0 at the preload stage and drops after the construction is completed and the strength of the outer RC develops. Furthermore, $N_{CFST}/N_{CE\text{-}CFST}$ drops by 4.7% within the sustained service load stage due to the load redistribution between concrete and steel. These phenomena do not exist in the full-range $N_{CFST}/N_{CE\text{-}CFST}$ development when short-termly loaded, as shown in Fig. 11(b2). It is also worth noting that the deformation ε_u for the column under combined loading is much larger than that subjected to short-term load, as exhibited in Figs. 11(a1) and (b1), which is consistent with the observation in Fig. 8.

3.3 Steel-concrete material interaction

The composite cross-sectional capacity is highly related to the steel-concrete material interaction. In a concrete-encased CFST, the material interaction greatly affects the load-transferring mechanism and eventually, the load-carrying capacity. To reveal the confinement effects between different contact pairs, the full-range development of the contact stress (p) between the concrete core and the steel tube, as well as that between the outer concrete and the steel tube, are presented in Fig. 12 for the composite column with construction preload on inner CFST followed by sustained service load over the entire composite section and a reference one subjected to short-term load only. Furthermore, Fig. 13 gives schematic illustrations of the material interaction along the composite cross-section at selected characteristic occasions during the loading process. As can be seen from both figures, due to the complex structural configuration and loading sequence, the material interaction in a concrete-encased CFST column is complex and dynamic during the full-range loading.

At the preload stage, both Fig. 12(a) and Fig. 13(a) show no contact (normal) stress exists between steel and concrete in the inner CFST. This is attributed to the fact that the Poisson's ratio of steel is larger than that of concrete in the elastic stage, inducing separation between the tube and its core concrete and therefore no contact stress under preload. For the same reason, when service load is applied, the smaller Poisson's ratio of the outer concrete leads to a smaller lateral deformation than that of the tube, producing interaction stress between the outer concrete and the steel tube in the sustained loading stage, as can be found from Fig. 12(a) and Fig. 13(b). Then during the sustaining of the service load, the creep of outer concrete leads to larger lateral expansion and thus the decrease of its contact stress with the steel tube.

When the sectional capacity test initiates, as exhibited in Fig. 13(c), the contact stress between the outer concrete and

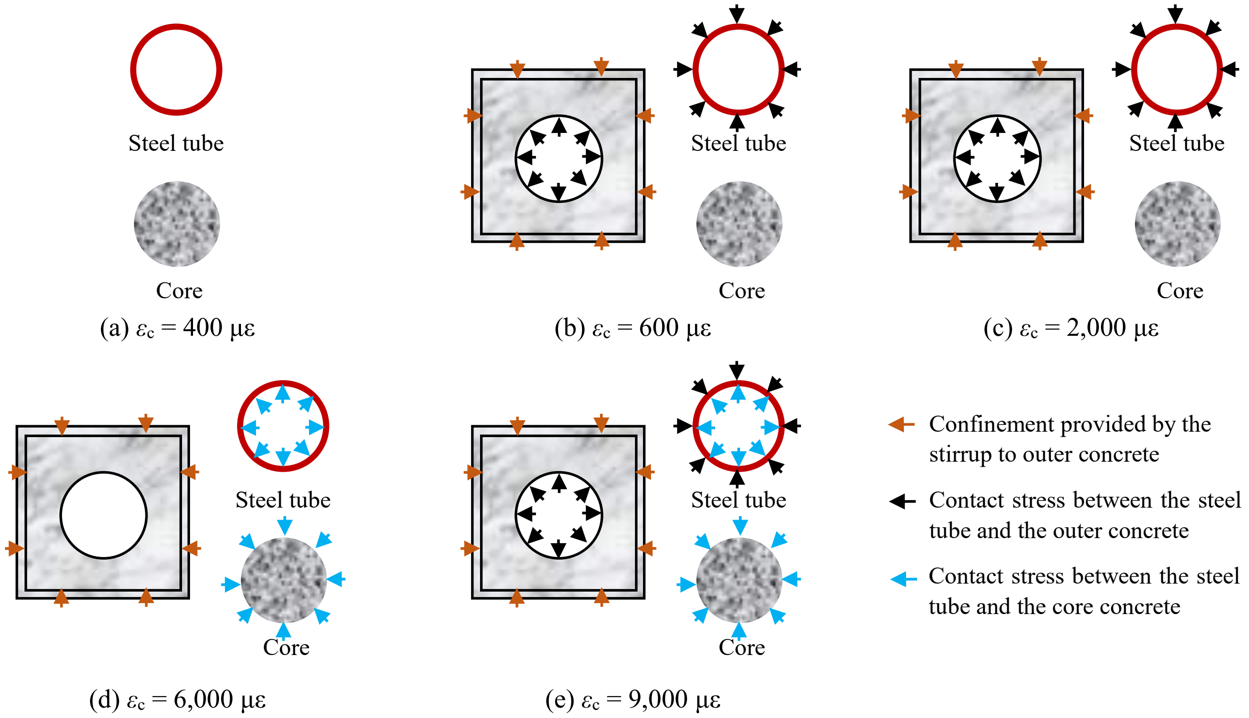

Fig. 13 Material interaction between steel and concrete at different loading stages

the steel tube is found to be 0.11 MPa whilst that of the contact pair concrete core-tube does not exist as explained above. With the increase of loading, the contact stress at the outer surface of the tube slightly drops to zero whilst that of the contact pair concrete core-tube starts to take place, as shown in Figs. 12(a) and 13(d). This happens because of the formation of the micro-cracks in the outer RC which greatly increases its lateral deformation when close to the ultimate strength. Therefore, the contact at the outer surface of the steel tube decreases whilst that at the inner surface develops as a result of the increased deformation of the concrete core. Afterwards, when the steel tube yields and local buckling occurs, the tube and the outer concrete recontact and the interaction stress is regenerated, as shown in the ending stage of the curve in Fig. 12(a) and the illustration in Fig. 13(e). This proves that when reaching the sectional capacity of a concrete-encased CFST column, effective confinement is detected between the steel tube and the concrete in both its outer and inner regions, leading to enhanced strength and ductility.

For both the two loading conditions, the interaction stresses of the contact pair concrete core-tube are much larger than those of the outer concrete-tube pair, as presented in Figs. 12(a) and 12(b). This attributes to the cracking of outer concrete after reaching the sectional capacity. The maximum contact stress is detected as around 3.45 MPa between the tube and its inner concrete. When reaching the sectional capacity of the composite column, the corresponding interaction stress between the concrete core and the steel tube is 1.57 MPa for the column under combined loading, while that of the short-termly loaded counterpart is 0.41 MPa. A larger contact stress is obtained when preload and sustained service load is applied since effective material interaction is induced by the load-redistribution along the composite cross-section caused by the combined loading.

4. Parametric analysis

To identify the impacts of key factors towards a concrete-encased CFST with construction preload followed by sustained service load, an extended parametric analysis is carried out using the developed FEA model. The influence of a set of selected parameters on the sectional capacity as well as the material interaction is evaluated and compared. Detailed information of the computational cases for the concrete-encased CFST columns are presented in Table 2. As can be observed, the varied parameters include: the strength of the outer concrete ($f_{cu,out}$), the strength of the concrete core ($f_{cu,core}$), the steel tube ratio of the composite section (α_s), the diameter to side length ratio (D/B), the above-defined construction preload ratio (n_p) and the sustained service load ratio (n_l). The influence of these parameters on the N-ε_c relationships is shown in Fig. 14, whilst the corresponding $N_{CFST}/N_{CE\text{-}CFST}$ versus ε_c relationships are exhibited in Fig. 15.

As has been found from the full-range load-strain relationship in Fig. 8, the combined construction preload and service load affect both the sectional capacity and the ductility of a concrete-encased CFST column. To quantify the influence of the combined load on the column ductility, a ductility index (DI) is adopted as follows

$$DI = \frac{\varepsilon_{85\%}}{\varepsilon_u} \tag{2}$$

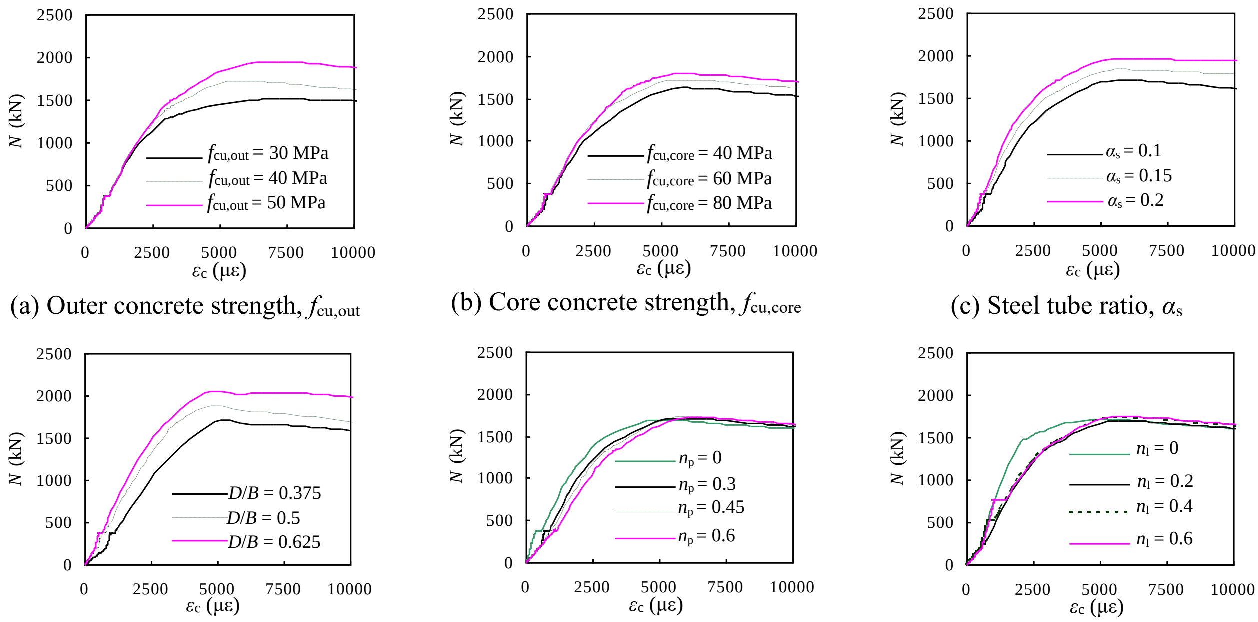

(a) Outer concrete strength, $f_{cu,out}$ (b) Core concrete strength, $f_{cu,core}$ (c) Steel tube ratio, α_s

(d) Cross-sectional configuration, D/B (e) Construction preload ratio, n_p (f) Sustained service load ratio, n_l

Fig. 14 Material interaction between steel and concrete at different loading stages

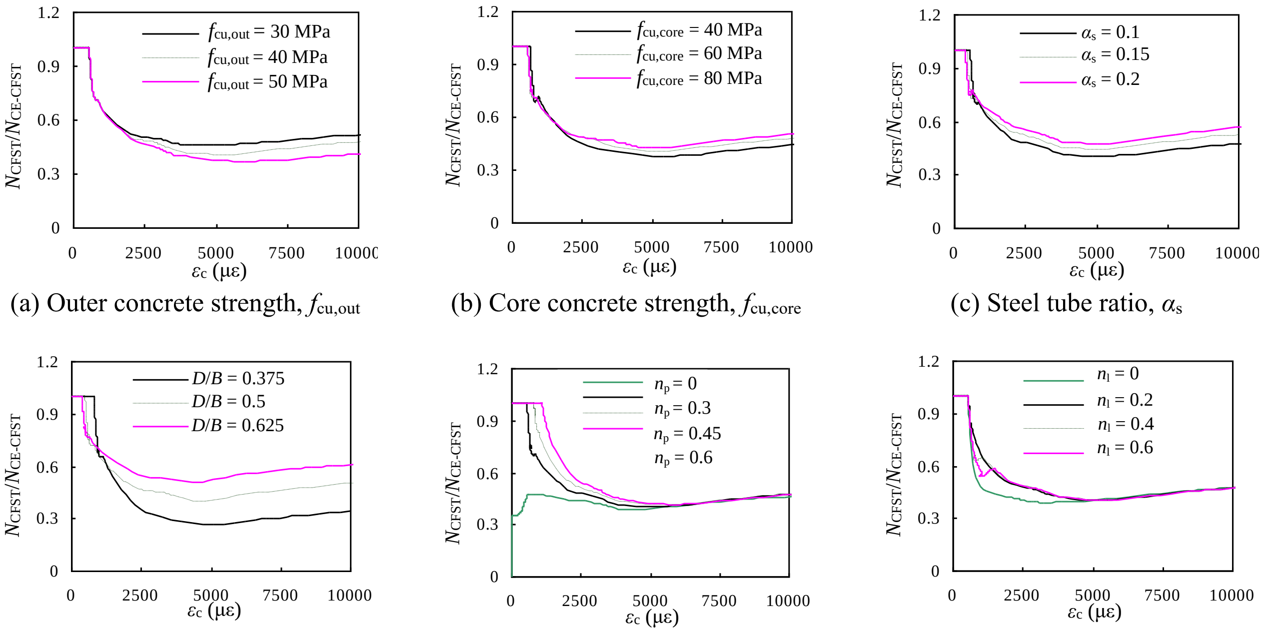

(a) Outer concrete strength, $f_{cu,out}$ (b) Core concrete strength, $f_{cu,core}$ (c) Steel tube ratio, α_s

(d) Cross-sectional configuration, D/B (e) Construction preload ratio, n_p (f) Sustained service load ratio, n_l

Fig. 15 Influence of different parameters on the development of $N_{CFST}/N_{CE\text{-}CFST}$ ratio

where $\varepsilon_{85\%}$ is the axial strain when the load drops to 85% of the column sectional capacity N_u under construction preload followed by sustained service load in the descending stage, and ε_u is the axial strain corresponding to the sectional capacity N_u. The influences of the above parameters on the defined *DI* are exhibited in Fig. 16.

4.1 Strength of the outer concrete ($f_{cu,out}$)

The strength of the outer concrete $f_{cu,out}$ is expected to have considerable influences on the sectional capacity of concrete-encased CFST since the outer RC contributes largely to the column capacity, as has been found in Fig. 11. It can be observed in Fig. 14(a) that $f_{cu,out}$ has a positive correlation with the sectional capacity of the analysed columns. With the designed axial load level being fixed, i.e., n_p = 0.3 and n_l = 0.3, the sectional capacity of the concrete-encased CFST columns increases by 28.9% when $f_{cu,out}$ increases from 30 to 50 MPa. Moreover, as $f_{cu,out}$ increases, $N_{CFST}/N_{CE\text{-}CFST}$ decreases in the sectional capacity test stage as presented in Fig. 15(a) since the outer RC component can sustain an increased proportion of the load.

Table 2 Information of the concrete-encased CFST cases in the parametric analysis

Specimen labels	Group	$f_{cu,outer}$ (MPa)	$f_{cu,core}$ (MPa)	α_s	D/B	n_p	n_l
s-1-a	Variation of $f_{cu,outer}$	30	60	0.1	0.5	0.3	0.3
s-1-b		40	60	0.1	0.5	0.3	0.3
s-1-c		50	60	0.1	0.5	0.3	0.3
s-2-a	Variation of $f_{cu,core}$	40	40	0.1	0.5	0.3	0.3
s-2-b		40	60	0.1	0.5	0.3	0.3
s-2-c		40	80	0.1	0.5	0.3	0.3
s-3-a	Variation of α_s	40	60	0.1	0.5	0.3	0.3
s-3-b		40	60	0.15	0.5	0.3	0.3
s-3-c		40	60	0.2	0.5	0.3	0.3
s-4-a	Variation of D/B	40	60	0.1	0.375	0.3	0.3
s-4-b		40	60	0.1	0.5	0.3	0.3
s-4-c		40	60	0.1	0.625	0.3	0.3
s-5-a	Variation of n_p	40	60	0.1	0.5	0.3	0.3
s-5-b		40	60	0.1	0.5	0.45	0.3
s-5-c		40	60	0.1	0.5	0.6	0.3
s-6-a	Variation of n_l	40	60	0.1	0.5	0.3	0.2
s-6-b		40	60	0.1	0.5	0.3	0.4
s-6-c		40	60	0.1	0.5	0.3	0.6

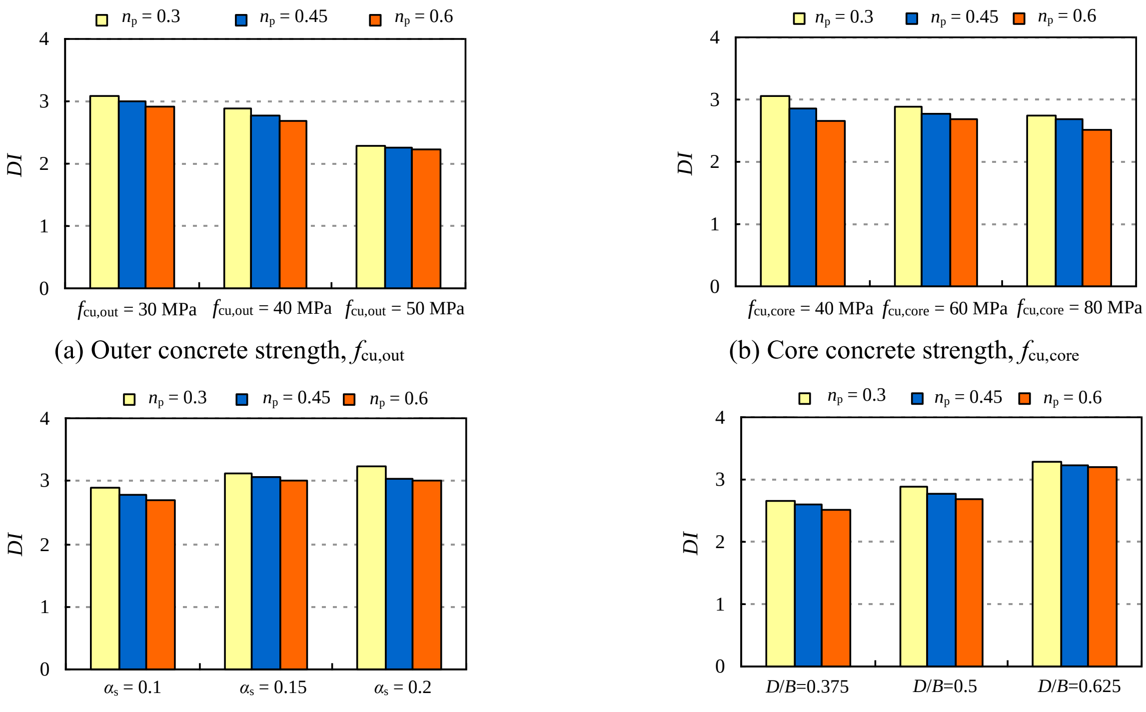

(a) Outer concrete strength, $f_{cu,out}$ (b) Core concrete strength, $f_{cu,core}$

(c) Steel tube ratio, α_s (d) Cross-sectional configuration, D/B

Fig. 16 Influence of different parameters on the ductility (DI)

The effects of $f_{cu,out}$ on DI are exhibited in Fig. 16(a). As can be seen, the growing $f_{cu,out}$ leads to a certain drop in the DI values. Meanwhile, for the commonly-used concrete strength $f_{cu,out}$ = 40 MPa, DI index decreases from 2.885 to 2.689 with the construction preload ratio increasing from 0.3 to 0.6.

4.2 Strength of the concrete core ($f_{cu,core}$)

The strength of the concrete core $f_{cu,core}$ is identified as another significant factor that governs the behaviour of a column under construction preload followed by sustained

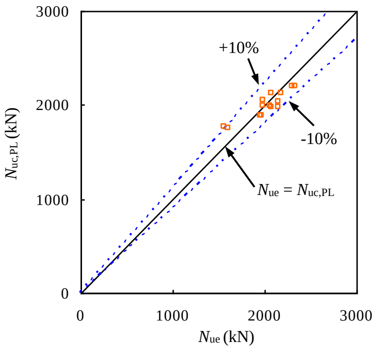

(a) Comparisons between $N_{uc,PL}$ and N_{ue}

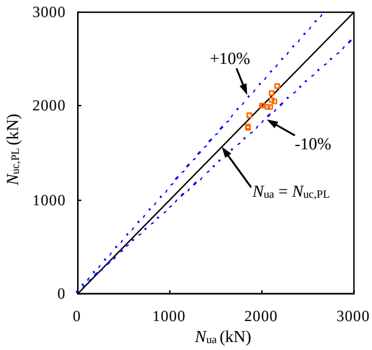

(b) Comparisons between $N_{uc,PL}$ and N_{ua}

Fig. 17 Comparison of the measured (N_{ue}), analyzed (N_{ua}) and calculated ($N_{uc,PL}$) sectional capacities

service load. With the increase of $f_{cu,core}$ from 40 to 80 MPa, the sectional capacity increases from 1,633.5 to 1,790.0 kN as presented in Fig. 14(b). Fig. 15(b) indicates that the increase in $f_{cu,core}$ leads to an increase in $N_{CFST}/N_{CE\text{-}CFST}$ ratio. When $f_{cu,core}$ increases from 40 to 80 MPa, the $N_{CFST}/N_{CE\text{-}CFST}$ ratio corresponding to the sectional capacity increases from 0.378 to 0.438. With different core concrete strength, DI index always decreases with the increase of the construction preload ratio. When the preload changes from 0.3 to 0.6 for specimens with $f_{cu,core}$ = 40 MPa, *DI* decreases from 3.051 to 2.661. For the frequently-used $f_{cu,core}$ = 60 MPa, the ductility index *DI* drops by 6.8% when the preload ratio n_p increases from 0.3 to 0.6.

4.3 Steel tube ratio (α_s)

The steel tube ratio α_s ($=A_s/A_{core}$) gives a geometric evaluation of the proportion of steel tube in the composite cross-section. It thus greatly affects the load-transferring mechanism and the sectional capacity of the column. Fig. 14(c) presents the influence of steel tube ratio α_s on the N-ε_c relationships of concrete-encased CFST columns subjected to combined loading, where the variation of steel tube ratio is achieved by changing the tubular thickness. Generally, the sectional capacity of the composite specimen increases with the increasing of α_s, as well as the variation trend of $N_{CFST}/N_{CE\text{-}CFST}$ versus axial strain relations shown in Fig. 15(c). When the steel tube ratio α_s grows from 0.1 to 0.2, the sectional capacity increases from 1,715.6 to 1,961.8 kN as shown in Fig. 14(c), and the $N_{CFST}/N_{CE\text{-}CFST}$ ratio corresponding to the ultimate strength increases by 21.9%. This attributes to the fact that an increased steel tube ratio leads to more effective confinement effects on the concrete core. Besides, the increase in steel tube ratio leads to an increase in the ductility index due to increased steel material in the cross-section, as presented in Fig. 16(c). On the other hand, a negative correlation between the preload ratio and the ductility index can be illustrated from Fig. 16(c). With preload ratio increases from 0.3 to 0.6, *DI* of the specimens with a steel tube ratio α_s = 0.1 decreases from 2.885 to 2.689, while it drops from 3.233 to 2.996 for specimens with α_s = 0.2.

4.4 Tube diameter to side length ratio (D/B)

The influence of tube diameter to side length ratio (D/B) on the N-ε_c relationships of concrete-encased CFST columns is exhibited in Fig. 14(d). The sectional capacity of composite specimens increases by 19.2% when D/B increases from 0.375 to 0.625. This is based on the fact that the enlarged D/B ratio leads to a larger area of the concrete core inside the steel tube under the direct confinement effect provided by the steel tube. The obvious effects of D/B ratio on $N_{CFST}/N_{CE\text{-}CFST}$ versus axial strain relationships can be observed in Fig. 15(d). As D/B increases from 0.375 to 0.625, the $N_{CFST}/N_{CE\text{-}CFST}$ value at the ultimate strength increases significantly from 0.268 to 0.577. This is well expected since an increasing D/B leads to larger dimensions of the inner CFST as well as the load resisted by the inner CFST. Fig. 16(d) displays the influence of D/B ratio on *DI*. The *DI* value always increases with the increase of D/B ratio while decreases with the increase of preload ratio n_p. For example, the *DI* of a column with D/B = 0.375 decreases by about 6% when np increases from 0.3 to 0.6.

4.5 Construction preload ratio (n_p)

The influence of the construction preload ratio n_p on the N-ε_c curves is presented in Fig. 14(e). The preload has only moderate effect on the sectional capacity of the composite columns, which is consistent with the observation in the companion experiment (Li *et al.* 2019). This attributes to the fact that the preload generally induces elastic behaviour of the inner CFST. However, as observed in Fig. 15(e), the existence of the preload greatly varies the load-carrying mechanism inside a concrete-encased CFST column. As n_p increases, $N_{CFST}/N_{CE\text{-}CFST}$ increases before the composite column reaching its ultimate strength, as exhibited in Fig. 15(e). Afterwards, the effect of preload ratio on the $N_{CFST}/N_{CE\text{-}CFST}$ ratio is not obvious. Compared with that on the column strength, the preload has larger effects on the column stiffness, as can be observed from Fig. 14(e). It is presented in Fig. 16 that the *DI* value of the specimens always decreases with the increase of the construction preload ratio n_p, which is another negative impact of the preload on the behaviour of such composite specimens.

4.6 Sustained service load ratio (n_l)

Fig. 14(f) presents the influence of the sustained service load ratio n_l on the N-ε_c relationships of concrete-encased CFST columns. It can be seen that n_l has a moderate effect on the sectional capacity of the column under the preload followed by sustained service load. The sectional capacity of the specimens increases with the increases of n_l, which is in accordance with the conclusion in Ma *et al.* (2018b). When n_l increases from 0.2 to 0.6, N_u slightly increases from 1,703 kN to 1,752 kN. On the contrary, the influence of sustained service load ratio towards the column stiffness is more significant, as shown in Fig. 14(f).

5. Prediction of the sectional capacity

The aforementioned research findings prove that the effects of preload followed by sustained service load on the performance of concrete-encased CFST cannot be ignored. Thus, rational consideration is required when predicting the sectional capacity of the composite column during design. Previously, preliminary discussions on the sectional capacity calculation for the concrete-encased CFST considering sustained loading and preload factors were presented in Ma *et al.* (2018b) and Li *et al.* (2019), respectively. On the basis of the full-range analysis and extended parametric study in the current paper, a simplified design formula to calculate the sectional capacity of concrete-encased CFST with construction preload followed by sustained service load is proposed through modification of the established method in Li *et al.* (2019) and Ma *et al.* (2018b), as expressed in Eq. (3). Generally, the bearing capacity of such a composite column is considered as two parts, namely, the RC part and the inner CFST part. Conventionally, the confinement in the inner CFST is accounted for, whilst the positive interaction between the inner CFST and the surrounding RC is not for conservative reasons. According to the numerical findings in regard of the detailed load-transfer mechanism, the method in the companion experimental study (Li *et al.* 2019) is modified, i.e., the preload effect is accounted for when calculating the strength of the inner CFST rather than the entire composite cross-section. This is in accordance with the actual construction sequence of a concrete-encased CFST column in practice, where the inner CFST component bears the construction preload individually.

$$N_{\mathrm{uc,PL}} = k_P N_{\mathrm{uc,CFST,L}} + N_{\mathrm{uc,RC,L}} \tag{3}$$

where $N_{\mathrm{uc,PL}}$ is the sectional capacity for a concrete-encased CFST member with construction preload on inner CFST followed by sustained service load on the entire cross-section; $N_{\mathrm{uc,CFST,L}}$ and $N_{\mathrm{uc,RC,L}}$ are the compressive capacities for individual inner CFST and outer RC parts considering the long-term effects, respectively; k_P is the strength index accounting for the preload influence on the inner CFST, which refers to Han and Yao (2003) and can be estimated as follows

$$k_{\mathrm{p}} = 1 - f(\lambda_0) f(e/r) n_{\mathrm{p}} \tag{4}$$

where n_{p} is the preload ratio; $f(e/r)$ = 0.9 for axial compression condition; $f(\lambda_0)$ defines a function taking into consideration the effects of the column slenderness λ_0 (Han and Yao 2003). For the current case, i.e., inner CFST with circular configurations, the function of $f(\lambda_0)$ becomes

$$f(\lambda_0) = \begin{cases} 0.17\lambda_0 - 0.02 & (\lambda_0 \le 1) \\ -0.13{\lambda_0}^2 + 0.35\lambda_0 - 0.07 & (\lambda_0 > 1) \end{cases} \tag{5}$$

The effects of the sustained service load upon the column sectional capacity are considered in the calculation of the compressive capacities for both the inner CFST and the outer RC components. $N_{\mathrm{uc,CFST,L}}$ and $N_{\mathrm{uc,RC,L}}$ in Eq. (3) are calculated as follows

$$N_{\mathrm{uc,CFST,L}} = k_{\mathrm{cr}} N_{\mathrm{uc,CFST}} \tag{6}$$

$$N_{\mathrm{uc,RC,L}} = \alpha_{\mathrm{cc}} N_{\mathrm{uc,RC}} \tag{7}$$

where $N_{\mathrm{uc,RC}}$ and $N_{\mathrm{uc,CFST}}$ are the compressive capacities of the outer RC the inner CFST parts, respectively. There are mature calculation methods for RC and CFST under axial compression in Eurocode 2 (2004) and DBJ/T13-51-2010 (2010). For the unfavorable influence of sustained service load on both the RC and the inner CFST parts, factors α_{cc} and k_{cr} related to material properties, column configuration and loading conditions are used in Eqs. (6) and (7), the values of which are determined in accordance with the methods described in Eurocode 2 (2004) and Han *et al.* (2004).

The predicted sectional capacities ($N_{\mathrm{uc,PL}}$) of concrete-encased CFST using the above method are compared against those measured (N_{ue}) in the companion experimental study (Li *et al.* 2019) and those analysed (N_{ua}) using the FEA models. The comparisons are exhibited in Table 1 and Fig. 17. The mean values for the ratios $N_{\mathrm{uc,PL}}/N_{\mathrm{ue}}$ and $N_{\mathrm{uc,PL}}/N_{\mathrm{ua}}$ are obtained to be 0.996 and 0.985, respectively, with the standard deviations of 0.040 and 0.058. Therefore, the sectional capacity of the entire composite columns with construction preload on inner CFST followed by sustained service load on the entire cross-section can be estimated by using the above formulas with good accuracy while being reasonably conservative.

6. Conclusions

On the basis of the companion experimental studies in Li *et al.* (2019), the current paper further investigates the full-range behaviour of concrete-encased CFST columns with construction preload on the inner CFST followed by sustained service load on the entire cross-section through a comprehensive numerical framework. The following conclusions can be drawn,

- A FEA model is established for the full-range simulation of concrete-encased CFST subjected to construction preload followed by sustained service load. Advanced modelling techniques are adopted to reproduce the actual construction stages and loading sequence for such composite columns. The varied material interaction between steel and concrete in different regions of the column are specifically taken into account. The simulations of the FEA model agree well with the experiments in terms of the sectional capacity, the failure pattern and the load-strain development.

- Full-range numerical analysis on concrete-encased CFST under construction preload followed by sustained service load is conducted by using the verified FEA model. It can be indicated that the combined loading has considerable influence on the load-strain characteristic, the stress developments, the internal force distribution and the contact stress along the interfaces. With construction preload and sustained service load, the load-strain behaviour is described as four stages, and effective material interaction is observed at both surfaces of the steel tube when the ultimate strength is approached.

- The extended parametric study show that $f_{cu,out}$, α_s, n_p and D/B have considerable influence on the load-strain relationship, the internal load distribution and the ductility of a concrete-encased CFST specimen, among which the D/B ratio has the most significant effects. It is suggested that relatively larger inner CFST dimensions together with higher-strength outer concrete can be regarded as an optimal design of the composite column. It is also certified in the current analysis that the preload ratio should be restrained within the suggested limitation of 0.6 in CECS 188:2008 (2005).

- A simplified design formula is proposed to calculate the sectional capacities of concrete-encased CFST columns under construction preload followed by sustained service load aided by existing design guidelines such as Eurocode 2 (2004) and DBJ/T13-51-2010 (2010). Based on the actual construction procedure and the numerical findings in this paper, the influence of preload is reflected by a strength index on the inner CFST only. Accurate predictions with reasonable conservation are achieved.

Acknowledgments

The current research is part of the Project 51678341 supported by the National Natural Science Foundation of China (NSFC). The financial support is highly appreciated.

References

Attard, M. and Setunge, S. (1996), "Stress-strain relationship of confined and unconfined concrete", *ACI Mater. J.*, **93**(5), 432-442. https://doi.org/10.1016/j.engstruct.2012.03.027.

ABAQUS (2016), ABAQUS Standard User's Manual, version 6.16. Providence, RI, (USA): Dassault Systèmes Corp.

Campian, C., Nagy, Z. and Pop, M. (2015), "Behavior of fully encased steel-concrete composite columns subjected to monotonic and cyclic loading", *Procedia Eng.*, **117**, 439-451. https://doi.org/10.1016/j.proeng.2015.08.193.

CECS 188:2005 (2005), Technical specification for steel tube-reinforced concrete column structure, China Association for Engineering Construction Standardization; Beijing, China.

Chen, Z.Y., Zhao, G.F., Yi, W.J. and Lin, L.Y. (2002), "Experimental research on behavior of high strength concrete column reinforced with concrete-filled steel tube under axial compression", *J. Dalian Univ. Technol.*, **45**(5), 687-691. [in Chinese]

Chu, K.H. and Carreira, D.J. (1986), "Time-dependent cyclic deflection in R/C beams", *J. Struct. Eng.*, 112(5), 943-959. https://doi.org/10.1061/(ASCE)0733-9445(1986)112:5(943).

DBJ/T13-51-2010 (2010), Technical specification for concrete-filled steel tubular structures, The Construction Department of Fujian Province; Fuzhou, China. [in Chinese]

Eurocode 2 (2004), Design of concrete structures-part 1-1: general rules and rules for buildings, European Committee for Standardization; Brussels, Belgium.

Han, L.H., Li, W. and Bjorhovde, R. (2014), "Developments and advanced applications of concrete-filled steel tubular (CFST) structures: Members", *J. Constr. Steel Res.*, **100**, 211-228. https://doi.org/10.1016/j.jcsr.2014.04.016.

Han, L.H. and An, Y.F. (2014), "Performance of concrete-encased CFST stub columns under axial compression", *J. Constr. Steel Res.*, 93, 62-76. https://doi.org/10.1016/j.jcsr.2013.10.019.

Han, L.H., Wang, Z.B., Xu, W. and Tao, Z. (2016), "Behaviour of concrete-encased CFST members under axial tension", *J. Struct. Eng. – ASCE*, **142**(2). https://doi.org/10.1061/(ASCE)ST.1943-541X.0001422.

Han, L.H. and Yao, G.H. (2003), "Behaviour of concrete-filled hollow structural steel (HSS) columns with pre-load on the steel tubes", *J. Constr. Steel Res.*, **59**(12), 1455-1475. https://doi.org/10.1016/S0143-974X(03)00102-0.

Han, L.H., Li, Y.J. and Liao, F.Y. (2011), "Concrete-filled double skin steel tubular (CFDST) columns subjected to long-term sustained loading". *Thin-Wall. Struct.*, **49**(12), 1534-1543. https://doi.org/10.1016/j.tws.2011.08.001.

Han, L.H., Yao, G.H. and Tao, Z. (2007), "Performance of concrete-filled thin-walled steel tubes under pure torsion". *Thin-Wall. Struct.*, 45(1), 24-36. https://doi.org/10.1016/j.tws.2007.01.008.

Han, L.H., Tao, Z. and Liu, W. (2004), "Effects of sustained load on concrete-filled hollow structural steel columns", *J. Struct. Eng.*, **130**(9), 1392-1404. https://doi.org/10.1061/(ASCE)0733-9445(2004)130:9(1392).

Hillerborg, A., Modéer, M. and Petersson, P.E. (1976), "Analysis of crack formation and crack growth in concrete by means of fracture mechanics and finite elements", *Cement Concrete Res.*, **6**(6), 773-782. https://doi.org/10.1016/0008-8846(76)90007-7.

Ichinose, L.H., Watanabe, E. and Nakai, H. (2001), "An experimental study on creep of concrete filled steel pipes". *J. Constr. Steel Res.*, **57**(4), 453-466. https://doi.org/10.1016/S0143-974X(00)00021-3.

Kang, L., Leon, R.T. and Lu, X.L. (2015), "Shear strength analyses of internal diaphragm connections to CFT columns", *Steel Compos. Struct.*, **18**(5), 1083-1101. https://doi.org/10.12989/scs.2015.18.5.1083.

Lam, D. and Williams, C.A. (2004), "Experimental study on concrete filled square hollow sections", *Steel Compos. Struct.*, 4(2), 95-112. https://doi.org/10.12989/scs.2004.4.2.095.

Li, S., Han, L.H. and Hou, C. (2018), "Concrete-encased CFST columns under combined compression and torsion: Analytical behaviour", *J. Constr. Steel Res.*, **144**, 236-252. https://doi.org/10.1016/j.jcsr.2018.01.020.

Li, Y.J., Li, G., Hou, C. and Zhang, W.J. (2019), "Long-term experimental behaviour of concrete-encased CFST with preload on the inner CFST", *J. Constr. Steel Res.*, **155**, 355-369. https://doi.org/10.1016/j.jcsr.2019.01.001.

Li, W., Han, L.H. and Zhao, X.L. (2015), "Behavior of CFDST stub columns under preload, sustained load and chloride corrosion", *J. Constr. Steel Res.*, **107**, 12-23. https://doi.org/10.1016/j.jcsr.2014.12.023.

Li, W., Han, L.H. and Zhao, X.L. (2012), "Axial strength of concrete-filled double skin steel tubular (CFDST) columns with preload on steel tubes", *Thin-Wall. Struct.*, **56**, 9-20. https://doi.org/10.1016/j.tws.2012.03.004.

Liew, J.Y.R. and Xiong, D.X. (2009), "Effect of preload on the axial capacity of concrete-filled composite columns", *J. Constr. Steel Res.*, **65**(3), 709-722. https://doi.org/10.1016/j.jcsr.2008.03.023.

Ma, D.Y., Han, L.H. and Zhao, X.L. (2019), "Seismic performance of concrete-encased CFST column to RC beam joint: Experiment", *J. Constr. Steel Res.*, **154**, 134-148. https://doi.org/10.1016/j.jcsr.2018.11.030.

Ma, D.Y., Han, L.H., Li, W. and Zhao, X.L. (2018a), "Seismic performance of concrete-encased CFST piers: analysis", *J. Bridge Eng.*, **23**(1), 04017119. https://doi.org/10.1061/(ASCE)BE.1943-5592.0001157.

Ma, D.Y., Han, L.H., Li, W., Hou, C. and Mu, T.M. (2018b), "Behaviour of concrete-encased CFST stub columns subjected to long-term sustained loading", *J. Constr. Steel Res.*, **151**, 58-69. https://doi.org/10.1016/j.jcsr.2018.09.016.

Roeder, C.W., Cameron, B. and Brown, C.B. (1999), "Composite action in concrete filled tubes", *J. Struct. Eng.*, **125**(5), 477-484. https://doi.org/10.1061/(ASCE)0733-9445(1999)125:5(477).

Uy, B. and Das, S. (1997), "Wet concrete loading of thin-walled steel box columns during the construction of a tall building"., *J. Constr. Steel Res.*, **42**, 95-119. https://doi.org/10.1016/S0143-974X(97)00022-9.

Varma, A.H., Ricles, J.M., Sause, R. and Lu, L.W. (2002), "Experimental behavior of high strength square concrete-filled steel tube beam-columns", *J. Struct. Eng. – ASCE*, **128**(3), 309-318. https://doi.org/10.1061/(ASCE)0733-9445(2002)128:3(309).

Wu, X.G., Zhao, X.Y. and Han, S.M. (2012), "Structural analysis of circular UHPCC form for hybrid pier under construction loads", *Steel Compos. Struct.*, **12**(2), 167-181. https://doi.org/10.12989/scs.2012.12.2.167.

Yang, M.G., Cai, C.S. and Chen, Y. (2015), "Creep performance of concrete-filled steel tubular (CFST) columns and applications to a CFST arch bridge", *Steel Compos. Struct.*, **19**(1), 111-129. https://doi.org/10.12989/scs.2015.19.1.111.

Zhang, Y.Y., Pei, J.N., Hunag, Y., Lei, K., Song, J. and Zhang, Q.L. (2018), "Seismic behaviors of ring beams joints of steel tube-reinforced concrete column structure", *Steel Compos. Struct.*, **27**(4), 417-426. https://doi.org/10.12989/scs.2018.27.4.417.

Zhou, K. and Han, L.H. (2018), "Experimental performance of concrete-encased CFST columns subjected to full-range fire including heating and cooling", *Eng. Struct.*, 165, 331-348. https://doi.org/10.1016/j.engstruct.2018.03.042.

BL